Journal of Nano- and Electronic Physics
Vol. **8** No 4(2), 04058(8pp) (2016)

Журнал нано- та електронної фізики
Том **8** № 4(2), 04058(8cc) (2016)

An Investigation of High Performance Heterojunction Silicon Solar Cell Based on *n*-type Si Substrate

N. Memarian*, M. Minbashi, M. Jalali Mehrabad

Faculty of Physics, Semnan University, 35131-19111 Semnan, Iran

(Received 28 July 2016; published online 23 December 2016)

In this study, high efficient heterojunction crystalline silicon solar cells without using an intrinsic layer were systematically investigated. The effect of various parameters such as work function of transparent conductive oxide (ϕ_{TCO}), density of interface defects, emitter and crystalline silicon thickness on heterojunction silicon solar cell performance was studied. In addition, the effect of band bending and internal electric field on solar cell performance together with the dependency of cell performance on work function and reflectance of the back contact were investigated in full details. The optimum values of the solar cell properties for the highest efficiency are presented based on the results of the current study. The results represent a complete set of optimum values for a heterojunction solar cell with high efficiency up to the 24.1 % with V_{OC} = 0.87 V and J_{SC} = 32.69 mA·cm^{-2}.

Keywords: Heterojunction silicon solar cell, Numerical simulation, AMPS-1D, Work function optimization.

DOI: 10.21272/jnep.8(4(2)).04058 PACS numbers: 73.40.Lq, 78.20.Bh, 84.60.Jt

1. INTRODUCTION

The amorphous/crystalline heterojunction silicon solar cells have dragged massive interest in recent studies due to their high energy conversion efficiency, great stability and other beneficial mechanical properties [1]. The high-quality performance of these devices has been utilized in laboratory cells and over in mass production cells based on textured n-type crystalline silicon (C-Si) [2, 3]. In order to improve the efficiency of these solar cells, several experimental methods have been reported, such as thermal oxidation by silicon nitride plasma-enhanced chemical vapor deposition (PECVD), where the surface dangling bonds are passivated by oxygen or hydrogen atoms, respectively [4]. In addition, different cell structures such as passivated emitter rear locally diffused (PERL) cells, passivated emitter rear totally diffused (PERT) cells and passivated emitter and rear (PERC) cells, have been developed to achieve high efficiencies at UNSW (University of New South Wales) [1].

Alternatively, Sanyo Ltd. has developed a silicon solar cell called Heterojunction with intrinsic thin layer (HIT) cell, by inserting a very thin intrinsic a-Si:H layer between p-type and n-type Silicon layers, with the purpose of reducing the carrier recombination and defect density of states at the interface. Using this strategy, they have successfully achieved efficiencies over 22 % in laboratory cells and over 20 % in mass production cells based on textured *n*-type C-Si [1, 4].

To achieve high efficiency solar cells, there are several crucial parameters that need to be optimized. Using simulation programs and numerical analysis, it is possible to examine the influence of different parameters, which are whether highly unlikely be determined experimentally or, in most cases, the experiments would be extremely time-consuming, not to mention the financial costs. In order to address these concerns, beside the experimental researches, there are several simulation software and numerical solution packages which have been used widely by researchers, such as PC-1D (One-dimensional semiconductor device simulator), AMPS-1D (One-dimensional Analysis of Microelectronic and Photonic Structures), SCAPS (a Solar Cell Capacitance Simulator), ASA (Amorphous Semiconductor Analysis), AFORS-HET (Automat For Simulation of Heterostructures), SimWindows, ADEPT-F, ASPIN, etc. Many of these packages are dedicated to study Si solar cells, some are used to investigate thin film CIGS solar cells and others are for both as well as general electronics and PV devices [5]. Among these simulation packages, AMPS-1D is a powerful one and also has a user-friendly framework.

AMPS-1D is a general computer simulation code for designing and analyzing two terminal structures [6] to calculate various transport properties of different device structures such as *p*-*n* and *p*-*i*-*n* homo- and heterojunctions [7], *p*-*i*-*p* and *n*-*i*-*n* structures [8, 9], multijunction [10, 11] and Schottky barrier devices. These devices may have poly-crystalline, amorphous or single crystal layers or a combination of both [12]. However, the heterojunctions of crystalline and amorphous layers have to be dealt with more consideration because AMPS-1D does not provide an explicit model for carrier recombination at this kind of interfaces.

As it was mentioned, inserting a very thin intrinsic layer at the *p*-*n* interface can improve cell performance by defects passivation. However, it has been found that the P^+ a-SiC:H /n^+ poly-Si solar cell has higher conversion efficiency than the P^+ a-SiC:H/ *I* /n^+ poly-Si solar cell. The reported efficiencies for the best cells are around 17.4 % [13] and 19 % [14]. Therefore, the purpose of this paper is to simulate heterojunction amorphous/crystalline Si solar cell without intrinsic thin amorphous layer with AMPS-1D. Another important point is that, most of the researchers concentrate the exploitation of HIT solar cells on p-type C-Si substrates, since *p*-type C-Si substrates are more broadly

* n.memarian@semnan.ac.ir

used in current photovoltaic market [15, 16], although it has been reported that *a*-Si:H(*p*)/*c*-Si(*n*)/*a*-S:H(n^+) structure has higher efficiency than Si:H(*n*)/*c*-Si(*p*)/*a*-Si:H(p^+) heterojunction solar cell (19.8 % and 17.4 % respectively) [17]. Hence, in this work, we have selected the n-type crystalline Si substrate for the cell structure. A detailed investigation of cell parameters using AMPS package provides a better understanding of the role of each layer and main parameters that control the behavior of PV devices.

2. SOLAR CELL STRUCTURE AND NUMERICAL SIMULATION

The simulated cell schematic structure is presented in Fig. 1. It consists of TCO/ *a*-Si:H (*p*)/*c*-Si(*n*)/*a*-S:H(n^+)-BSF/ back contact. The data within the Fig. 1 is the optimum value for each layer. Since AMPS-1D does not provide an explicit model for carrier recombination at heterojunction interfaces, we have addressed this issue by inserting an artificial, extremely thin layer with a high bulk density of states representing the interface between the amorphous and crystalline silicon. It has been reported that, without the assistance of the back surface field (BSF) layer for minority carrier collection, most of the photo-generated electrons would be wasted at the back recombination sink [18]; therefore, a very thin n^+- BSF is subjected on the back side. The resistivity of the crystalline silicon set as 1.5 Ω cm. The electrons and holes surface recombination velocities were set as 1×10^7 cm/s. The main parameters of each layer used in the simulations are listed in Table 1. A 1.5 AM solar radiation with the power density of 100 mW/cm² are used as the source of illumination. The reflection of light at the front face (RF) was set at 0.01. For retro-reflection (RB) of the back contact, we used different values for the materials as listed in Table 2. The light absorption coefficient, for the different layers was already incorporated in the AMPS-1D program [19].

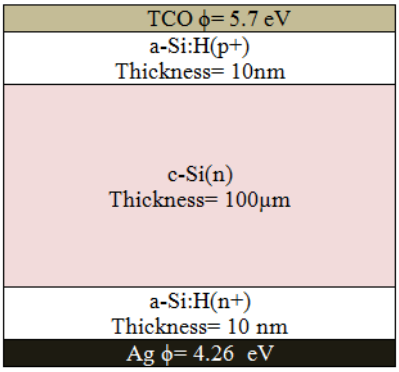

Fig. 1 – Schematic figure of the heterojunction amorphous/ crystalline silicon solar cell structure

The AMPS-1D program solves Poisson's equation coupled to electrons and holes continuity equations at each position throughout the device by taking into account the boundary conditions and using finite differences and the Newton- Raphson methods [6]. The program simulates device operation by taking into account the Shockley-Read-Hall recombination statistics [20]. The numerical simulation requires a model of the density of states (DOS) in each layer. In this work, it has been assumed that there are both exponential Urbach tail states and Gaussian-shaped midgap states. The tail states consist of both donor tail coming out of the valence band and an acceptor tail coming out of the conduction band, which are given as follows:

$$g_D(E) = G_{DO} \exp\left(\frac{E_V - E}{E_D}\right) \quad (2.1)$$

$$g_A(E) = G_{AO} \exp\left(\frac{E - E_C}{E_A}\right) \quad (2.2)$$

Where $G_{DO}(E)$ and $G_{AO}(E)$ are the densities per energy range for tail states at the band edge energies E_V and E_C, respectively; and E_A and E_D are characteristic parameters for the conduction and valence band tail states, respectively. Mid gap density of states, for the interface of hetrojunctions, acts as the interface density of state. The mid-gap states are described by Gaussian distributions of acceptor-like states and donor-like states:

$$g_A(E) = N_{AG} \exp\left\{\frac{-1}{2}\left[\frac{(E - E_{ACPG})^2}{W_{DSAG}^2}\right]\right\} \quad (2.3)$$

$$g_D(E) = N_{DG} \exp\left\{\frac{-1}{2}\left[\frac{(E - E_{DONG})^2}{W_{DSDG}^2}\right]\right\} \quad (2.4)$$

Where N_{AG} and N_{DG} are the density of states, E_{ACPG} and E_{DONG} are the peak energy position and W_{DSAG} and W_{DSDG} are the standard deviation of the Gaussian acceptor and donor levels, respectively. Detailed study on these parameters can be found elsewhere [1].

3. RESULTS AND DISCUSSION

3.1 Effect of Front Contact Work Function

TCOs have relatively high work functions of about 4-6 eV as well as high optical transparency in visible region. The work function of ITO has been reported ranging from 4.17 to 5.54 eV [21] and for FTO 4.48-5.35 eV [22]. Recently, new TCOs like WO_3/Ag/WO_3 (WAW) with high work function of about 5.2-6.2 eV have been reported [23]. It is very important to determine the proper work function for the front contact of a solar cell. So, it is necessary to simulate the influence of front contact work function on the cell performance. The results of functional properties (V_{OC}: open circuit voltage, J_{SC}: short circuit current, FF: fill factor and η: conversion efficiency) for simulated a-Si: H (p^+)/ *c*-Si (*n*) solar cell as a function of front contact work function are shown in the Figure 2.

The results show that by increasing the work function of front contact, the cell performance improves. From Fig. 2, it is clear that at $\phi_{TCO} = 4.7$ eV, the cell has a low performance with $\eta = 15.574$ %, $FF = 0.673$, $V_{OC} = 0.718$ V, $J_{SC} = 32.213$ mA/cm².

Table 1 – Parameter set for the simulation of the heterojunction solar cells

Parameter and units *e*, *h* for electrons and holes respectively	a-Si:H(p^+)	Interface at a-Si:H/*c*-Si	*c*-Si(*n*)	a-Si:H(n^+)
Thickness (nm)	3-18 (variable)	3	1000-400000 (variable)	10
Electron affinity (eV)	3.8	4.05	4.05	3.8
Band gap (eV)	1.72	1.12	1.12	1.72
Effective conduction band density (cm^{-3})	2.50×10^{20}	2.80×10^{19}	2.80×10^{19}	2.50×10^{20}
Effective valence band density (cm^{-3})	2.50×10^{20}	1.04×10^{19}	1.04×10^{19}	2.50×10^{20}
Electron mobility ($cm^2\ V^{-1}\ s^{-1}$)	10	1350	1350	10
Hole mobility ($cm^2\ V^{-1}\ s^{-1}$)	1	450	450	1
Doping concentration of acceptors (cm^{-3})	3×10^{19}	0	0	0
Doping concentration of donors (cm^{-3})	0	3×10^{15}	3×10^{15}	1×10^{20}
Band tail density of states ($cm^{-3}\ eV^{-1}$)	2×10^{21}	1×10^{14}	1×10^{14}	2×10^{21}
Characteristic energy (eV) donors, acceptors	0.06, 0.03	0.01	0.01	0.06, 0.03
Capture cross section for donor states, *e*, *h*, (cm^2)	1×10^{-15}, 1×10^{-17}	1×10^{-15}, 1×10^{-17}	1×10^{-15}, 1×10^{-17}	1×10^{-15}, 1×10^{-17}
Capture cross section for acceptor states, *e*, *h*, (cm^2)	1×10^{-17}, 1×10^{-15}	1×10^{-17}, 1×10^{-15}	1×10^{-17}, 1×10^{-15}	1×10^{-17}, 1×10^{-15}
Gaussian density of states (cm-3)	8×10^{17}	0	0	8×10^{17}
Gaussian peak energy (eV) donors, acceptors	1.22, 0.70	0	0	1.22, 0.70
Standard deviation (eV)	0.23	0	0	0.23
Midgap density of states ($cm^{-3}\ eV^{-1}$)	0	1×10^{15}-5×10^{19} (variable)	1×10^{11}	0
Switch over energy (eV)	0	0.56	0.56	0

By increasing the work function of the front contact from 4.7 to 5 eV, the efficiency of the cell increases considerably. By further increasing the ϕ_{TCO}, the efficiency increases slowly until it is saturated and it reaches its maximum, 24.07 % when the work function of the front contact was 5.68 eV. In the same manner, when the work function was higher than 5 eV, V_{OC} showed a constant value, 0.877 V. Similarly, the fill factor showed a constant value of 0.842. The behavior of J_{SC} is different. For the front contact work function up to 5 eV, J_{SC} was almost constant. Suddenly, by increasing the work function to 5.3 and more, there was an increment in the J_{SC}, which will be investigated in detail at the following.

The current voltage (*J*-*V*) curves of the simulated solar cells with lowest and highest work function of front contact are shown in Figure 3. "*H*" represents the highest efficiency and the "*L*" represents the lowest efficiency, which regards to highest and lowest front contact work function, respectively.

As it can be seen from Fig. 3 (and 2) the work function of front contact affects the V_{OC}, and it has not so much impact on J_{SC}. The efficiency of the *H* mode solar cell is 24.07 % and for *L* mode is 15.56 %. The *H* mode represents the optimum parameters for the solar cell that we investigate in our work. Such behavior can be described by the internal electric field and energy band structure of the cell.

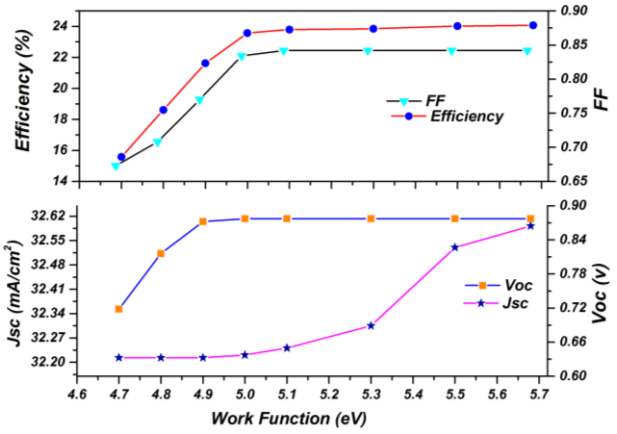

Fig. 2 – short circuit current, open circuit voltage, Fill Factor and efficiency variation as functions of front contact work function

For detailed study on the effect of front contact, we have focused on the electric field inside the cell. Figure 4 shows the electric field distribution of the proposed cell with illumination at 0 V, for two modes, (a) low front contact work function (*L* mode) and (b) for the high front contact work function (*H* mode). As one can see, with relatively low work function the electric filed is positive inside the TCO and near the TCO- P^+ Si interface, which hinders holes from reaching to the front electrode. For

high work function (Fig. 4b) the electric filed is negative inside the TCO and near the TCO- P^+ Si interface, which pushes holes toward the front electrode. At the same time, the strength of electric field in the space charge region (SCR) is almost the same for both modes.

Figure 5 shows the band diagram of the cell at thermodynamic equilibrium to investigate the band alignment and band offset.

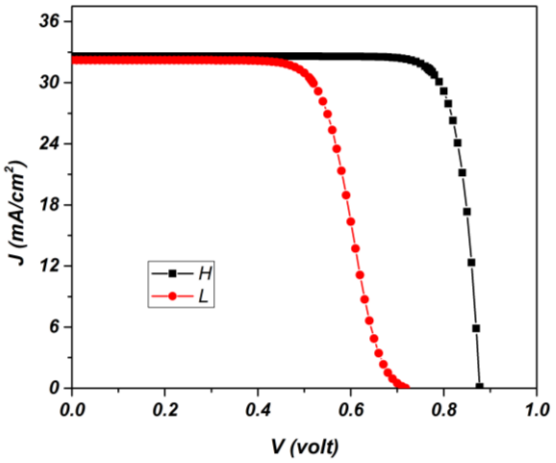

Fig. 3 – *J-V* Characteristic plots of the simulated solar cell at *H* and *L* Modes

The energy band structure of the cell with TCO work function of 4.7eV and 5.68eV are shown in figure 5 (a) and (b), respectively. χ_1 is the electron affinity. V_B is the build-in potential which is equal to the work function

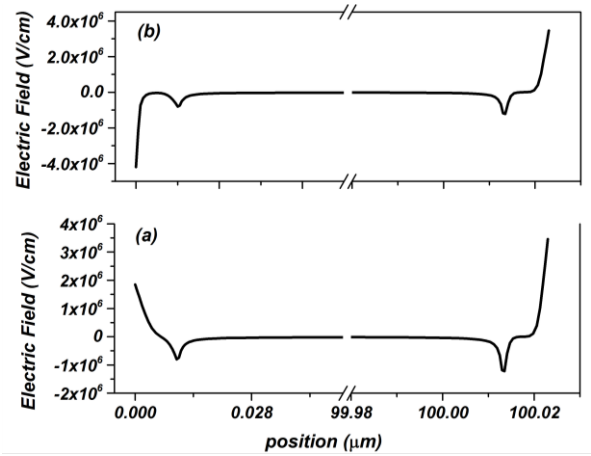

Fig. 4 – Electric Field variation as a function of position inside the cell, for (a) *L* and (b) *H* models

difference. Δ_v Valence band offset between two materials at a heterojunction. Φ_B is the energy difference between E_C and E_F for the *p*-type material.

From Fig. 5a, the front contact consists of a cliff about 0.5 eV at the conduction band of TCO/ p^+ interface. When work function of TCO is low, the Fermi energy level of TCO is higher than that of a-Si:H (p^+) layer, causing the holes to flow out of TCO layer into emitter layer. So both conduction and valence band reclined at the interface between TCO and emitter layer. In this way, the Schottky barrier of TCO/ a-Si:H (p^+) contact hinders the holes from forwarding to the front electrode; therefore, one can see a large abatement in the conversion efficiency.

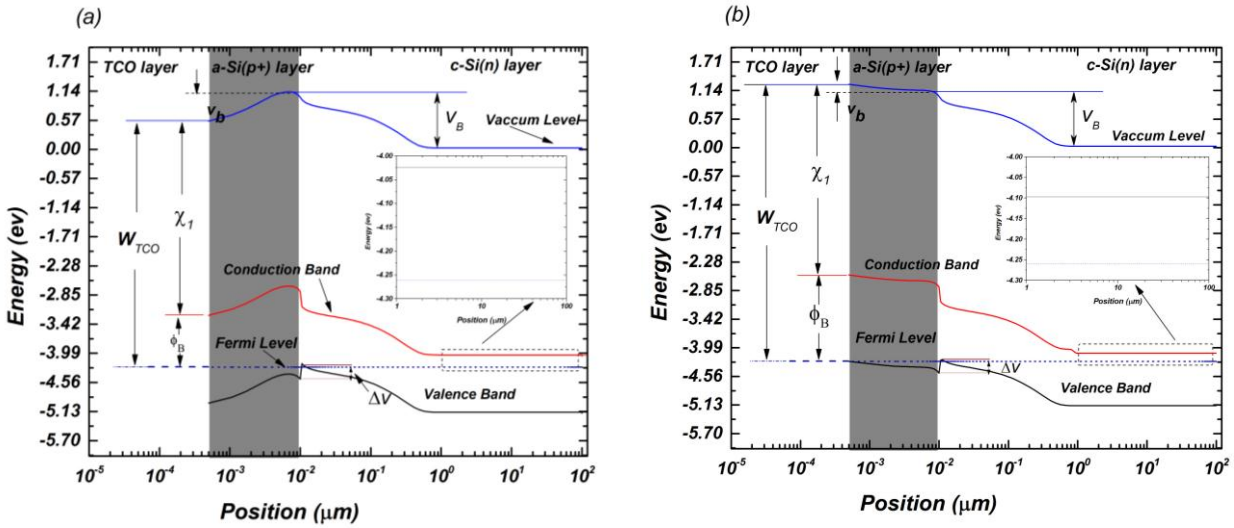

Fig. 5 – The energy band structure of the cell with different front contact work function (a) ϕ_{TCO} = 4.7 and (b) 5.68 eV, respectively

This can be avoided with more suitable TCO layer material with appropriate electron affinity and band gap or with new front contact material such as WAW. On the other hand, when the work function of TCO is relatively high, the Fermi energy level of this layer is equivalent to or less than that of emitter layer, which results in the holes flowing from emitter layer to the TCO. As shown in figure 5(b) both conduction and valence band bend atop at the interface between TCO and emitter layer, which shows the band offset at the TCO/ emitter interface does not act like a shottky contact and helps the generated holes flow to the front contact.

3.2 Study the Back Contact Work Function and Reflectance

In order to have a practical back contact, we have to pay attention to the issue of how to achieve a low resistance and small barrier height for back contact that are used in heterojunction solar cells. In order to find out

the impression of back contact work function on the functional parameters of P^+ a-Si:H/ n^+ C-Si heterojunction solar cell, the back contact work function varied from 3.8 to 4.53 eV, as listed in Table 2. Usually, the reflection coefficient of the back contact is considered as a constant parameter, while for a more realistic simulation, one has to consider that each material has different reflectance. For this purpose the reflectance of each material from references [24, 25] are also listed in Table 2. Recently ZnO:B has dragged a great attention due to its unique properties for application in solar cells. Films deposited by LPCVD technique have high reflectance (86 %) [24] and relatively low work function (3.8 eV) [26].

The simulation results of cell parameters versus back contact work function are shown in Figure 6 and given in Table 2. If the reflectance of all materials is considered the same, the results would be different and the best performance would have belonged to the cell with lowest back contact work function, while in the real situations the reflectance of each material is different. As it can be seen from the Figure 6 and Table 2, by increasing the back contact work function, the efficiency of the cell decreases. The V_{OC} remains constant, and J_{SC} has not an explicit trend. This is due to the effect of reflectance. So, the harsh reduction of efficiency, by increasing the back contact work function, is not just because of increase of work function. It is also because of decrease in reflectance of back contact.

This could be deduced directly from the efficiency and drift current equations as follow:

$$\eta = \frac{FF(J_{mp}V_{mp})}{P_{IN}} \qquad (3.1)$$

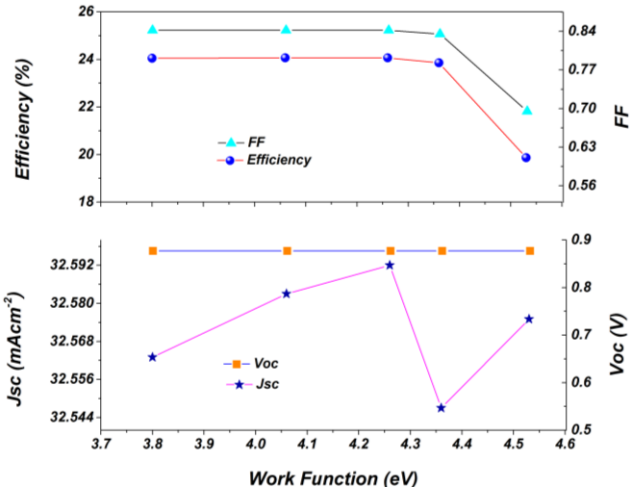

Fig. 6 – Short circuit current, open circuit voltage, Fill Factor and efficiency of the solar cell as functions of back contact work function

$$J_d(\lambda) = q\int_{x_j}^{x_j+w} g_E(\lambda)dx = q\alpha\varphi_0(1-R)e^{-\alpha x_j}\left(1-e^{-\alpha W}\right) \qquad (3.2)$$

Where α is the optical absorption coefficient, φ_0 is the incident photon flux density per unit bandwidth per second and R is the reflection coefficient [27]. The quantum efficiency can also be expressed by [28]:

$$QE = \frac{J_{sc}(\lambda)}{q\varphi_0(1-R)} \times 100\%, \qquad (3.3)$$

And Quantum efficiency is proportional to the cell efficiency. So it is clear that by increasing the reflectance, the efficiency also increases.

Table 2 – Back contact metal and cell functional parameters

Materials	ϕ (eV)	R	V_{OC} (V)	JSC (mA/cm²)	FF	Efficiency
ZnO:B	3.8	0.86 [24]	0.87	32.56	0.84	24.05
Al	4.06	0.93 [25]	0.87	32.58	0.84	24.06
Ag	4.26	0.96 [25]	0.87	32.59	0.84	24.07
Mo	4.36	0.80 [25]	0.87	32.55	0.83	23.85
Cu	4.53	0.90 [25]	0.87	32.57	0.69	19.87

3.3 Effect of Emitter Layer Thickness

The a-Si: H (p^+) layer is used as emitter layer in the simulated solar cell. Figure 7 shows the variation of cell performances in heterojunction configuration with the change of p-layer thickness in the range of 3-18 nm. According to the Fig. 7, as the a-Si (p^+) layer thickness increases, the efficiency of the cell decreases. The highest efficiency of 24.14 % has been achieved for this cell with the 3 nm thickness of the emitter. When the emitter thickness increases more than 8 nm, the cell efficiency decreases rapidly due to the reduction of the J_{SC}. Since by increasing the emitter thickness, the more photoelectrons undergo recombination and fewer amounts of them can reach to the electrode and transport loss become dominant. Ultra-thin absorber layer minimize recombination losses. In addition, the emitter thickness should be as thin as possible to allow maximum incident radiation passes through the cell and reach to the p-n junction. The best value of the efficiency is for 3 nm thickness. For more realistic statements, however, the thickness of 10 nm, which is possible to synthesize by molecular beam epitaxy (MBE) method, is used in our optimize model (24.07 % efficiency).

3.4 Effect of C-Si Layer Thickness

The simulation results for different values of C-Si (n) layer thickness are shown in figure 8. The thickness varied from 3 to 400 μm. Two main different trends can be recognized. It is clear from fig. 8 that as the layer thickness increases from 3 to 60 μm, the cell efficiency increases sharply, where V_{OC} remains constant and increase in J_{SC} results in higher cell efficiency. This could be attributed to the higher absorption of light and consequently higher photoelectron generation. Since the fill factor is conversely proportional to the J_{SC}, it is

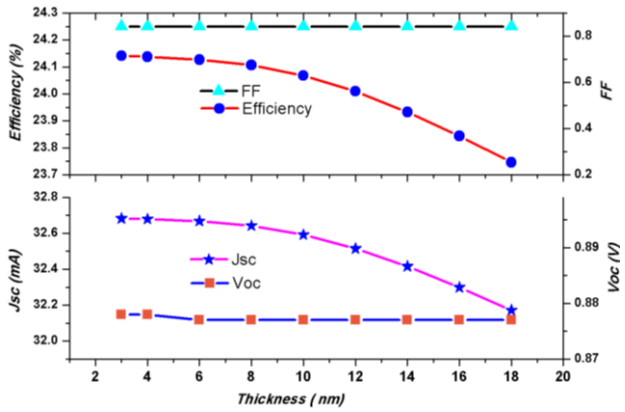

Fig. 7 – Short circuit current, open circuit voltage, Fill Factor and efficiency variation as functions of emitter thickness

obvious that by increasing the J_{SC} and V_{OC} remaining constant, the fill factor decreases. For higher C-Si thickness (more than 60 μm), the efficiency decreases slowly. As can be seen from fig. 8, J_{SC} remains almost constant but V_{OC} decreases.

Although from simulation results it seems that the thickness of 60 μm is the best thickness because of the highest efficiency, in real circumstances, in order to have a suitable wafer and avoiding cracks or breaking down the Si wafer, the *c*-Si (*n*) thickness should be at least 100 μm or higher. So the 100 μm is considered as the optimum value for the *n*-type crystalline Si wafer.

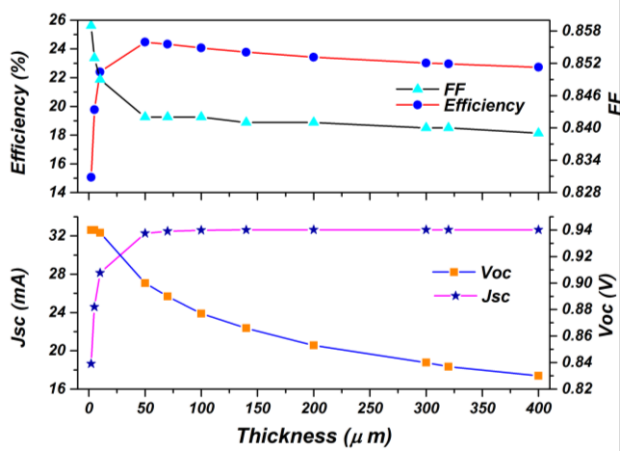

Fig. 8 – Short circuit current, open circuit voltage, Fill Factor and efficiency as functions of C-Si (*n*) thickness

3.5 Effect of Mid Gap Density of State

For high-efficiency heterojunction Si solar cells, the *c*-Si surface passivation is the most important factor [29]. Most commonly used approach to passivate the surface defects of *c*-Si and reduce interface carrier recombination is to use an intrinsic buffer layer. The passivation quality is crucial for the device open-circuit voltage (V_{OC}) and conversion efficiency.

To study the passivation effect on *c*-Si wafer, we considered an artificial interface layer at a-Si:H emitter - *c*-Si junction without considering any intrinsic layer. Study the mid gap density of states (DOS) allows the detection of trap energy levels. The simulation results of the mid gap density of states are shown in figure 9. The mid gap density of states varied from 4×10^{15} to 10^{20} $cm^{-3}v^{-1}$. As it can be seen from the Fig. 9, by increasing the mid gap density of states, the solar cell efficiency decreases. The highest efficiency is of $4\times10^{15}cm^{-3}v^{-1}$. For high density of mid gap states, interface recombination plays the dominant role and affects V_{OC} and can reduce it rapidly.

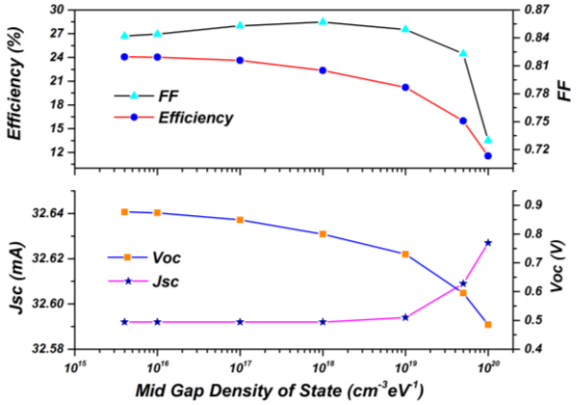

Fig. 9 – Short circuit current, open circuit voltage, Fill Factor and efficiency variation as functions of mid gap density of state

Here the decrease of the solar cell efficiency by increasing the mid gap DOS is attributed to the reduction of V_{OC}, although J_{SC} has a very small increase at higher midgap density of states. The whole passivation layer lies in the space charge region (SCR), and the recombination in SCR constitutes the device recombination current which causes negative effect on V_{OC} and efficiency [29].

For similar cells, it has been reported that the highest efficiency is 22 % [1], while here without using intrinsic layer we have obtained the efficiency around 24 %. Since the passivation of c-si is still an important factor, it is better to use different methods such as etching, plasma post-treatment and annealing processes as well as modifications of the wafer pre-cleaning procedure *c* to passivizing *p*-*n* interface and reducing the carrier recombination instead of buffer intrinsic layer.

3.6 Study of the Cell Quantum Efficiency

After optimization of different parameters, the quantum efficiency (QE) measurement for the simulated solar cell has been performed to evaluate the spectral response of the simulated solar cells, as shown in Figure 10. The variation of the QE versus incident light wavelength as functions of (a) front contact work function, (b) back contact work function, (c) mid gap density of states and (d) *c*-Si layer thickness are plotted. The QE curves show that the cell has a good spectral response in the wavelength range of 450 nm – 850 nm. Figure 10(a) illuminates that by increasing the front contact work function of solar cell, the QE at short wavelengths has increased. This reveals that such V_{OC} enhancement results from the increased light response to short wavelengths. The results show that the back contact work function has a small effect at

the high wavelength absorption. In addition variation of mid gap density of states has a low impact just on the short wavelengths quantum efficiency.

As it is clear from Fig. 10(d), increasing the thickness of the crystalline absorber layer has an explicit effect on the cell spectral response at long wavelengths, and the quantum efficiency at long wavelengths has increased significantly with increasing the P layer thickness. This is due to enhanced photon absorption, while for the thicknesses higher than 50 nm the change in QE is not as tangible.

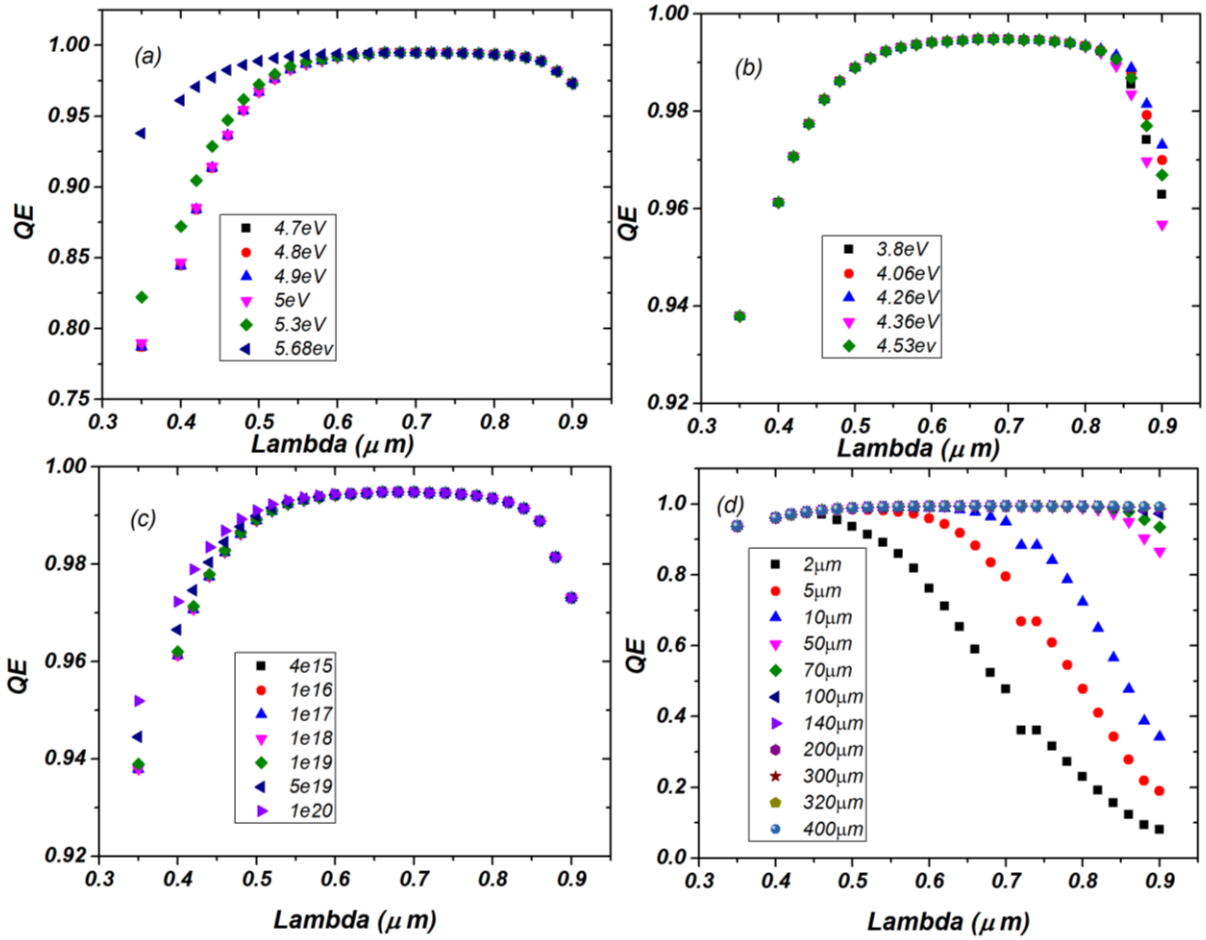

Fig. 10 – Quantum Efficiency variation as a function of (a) front contact work function, (b) back contact work function, (c) mid gap density of state and (d) C-Si layer thickness

4. CONCLUSION

In this paper, the AMPS-1D program was used successfully to study inorganic hetrojunction Si solar cell without intrinsic layer. The effects of different parameters on cell performance were systematically investigated. The results show that it is more convenient to use a TCO with high work function as a front contact of p^+/n heterojunction silicon solar cell. Detailed study reveals that both the work function and the reflectance of the back contact are important for choosing the optimum back contact material. The best cell performance belongs to the cell with highest back contact reflectance. By optimization the front contact work function, back contact reflectance and also without exerting intrinsic layer, we have achieved a high efficiency around 24.1%. So instead of using i layer, it is more practical to use optimized front and back contacts with appropriate work functions and reflectance. At the same time, different methods such as etching, plasma post-treatment and annealing processes as well as modifications of the wafer pre-cleaning procedure can be used to passivizing p-n interface and reducing the carrier recombination.

Moreover, by increasing the mid gap density of states, the solar cell efficiency decreases due to interface recombination. Finally the effects of each parameter on the spectral response were investigated from quantum efficiency simulation. The results show that the thickness of crystalline silicon wafer affects the high wavelength absorption.

AKNOWLEDGEMENTS

The authors would like to thank Professor S. Fonash of the Pennsylvania State University for providing the AMPS-1D program used in the simulations.

REFERENCES

1. N. Hernandez-Como, A. Morales-Acevedo, *Sol. Energ. Mater. Sol. C.* **94**, 62 (2010).
2. J. Zhao, *Sol. Energ. Mater. Sol. C.* **82**, 53 (2004).
3. M. Tanaka, S. Okamoto, S. Tsuge, S. Kiyama, *Third World Conference on Photovoltaic Energy Conversion*, 955, (Japan: 2003).
4. S. Taira, Y. Yoshimine, T. Baba, M. Taguchi, H. Kanno, T. Kinoshita, H. Sakata, E. Maruyama, M. Tanaka, *22nd European Photovoltaic Solar Energy Conference*, 932, (Italy: 2007).
5. M. Burgelman, J. Verschraegen, S. Degrave, P. Nollet, *Progress in Photovoltaics, Research and Applications*, **12**, 143 (2004).
6. S. Fonash, J. Arch., J. Cuiffi, J. Hou, W. Howland, P. McElheny, A. Moquin, M. Rogosky, T. Tran, H. Zhu, F. Rubinelli, *A Manual for AMPS-1D for Windows 95/ NT a One-Dimensional Device Simulation Program for the Analysis of Microelectronic and Photonic Structures* (The Pennsylvania State University: 1997).
7. M. Barrera, F. Rubinelli, I. Rey-Stolle, J. Pla, *Physica B* **407**, 3282 (2012).
8. A. Eray, G. Nobile, *Turk J Phys.* **28**, 31 (2004).
9. J.P.R. Bakker, B.J. van der Horst, J.I. Dijkhuis, *J. Non-Cryst. Solids* **299-302**, 1256 (2002).
10. A.A. Boussettine, Y. Belhadji, A. Benmansour, *Energy Procedia* **18**, 693 (2012).
11. B. Dennai, H. Ben Slimane, A. Helmaoui, *J. Nano- Electron. Phys.* **6** No 4, 04001 (2014).
12. L. Zhao, C.L. Zhou, H.L. Li, H.W. Diao, W.J. Wang, *Sol. Energ. Mater. Sol. C.* **92**, 673 (2008).
13. SH. Qing-Yi, Ch. A-Qing, Z. Kai-Gui, Z. Juan, *Chin. Phys. Lett.* **29**, 087302 (2012).
14. A. Bensmain, H. Tayoub, B. Zebentout, Z. Benamara, *Sensor. Transducer.* **27**, 82 (2014).
15. V. Dao, J. Heo, H. Choi, Y. Kim, S. Park, S. Jung, N. Lakshminarayan, J. Yi, *Sol. Energy* **84**, 777 (2010).
16. L. Zhao, H.L. Li, C.L. Zhou, H.W. Diao, W.J. Wang, *Sol. Energy* **83**, 812 (2009).
17. M. Schmidt, L. Korte, A. Laades, R. Stangl, Ch. Schubert, H. Angermann, E. Conrad, K.v. Maydell, *Thin Solid Films* **515**, 7475 (2007).
18. L.J.H. Lin, Y.P. Chiou, *Sol. Energy* **86**, 1485 (2012).
19. A. Belfar, B. Amiri, H. Ait-kaci, *J. Nano- Electron. Phys.* **7** No 2, 02007 (2015).
20. A. Bouloufa, K. Djessas, A. Zegadi, *Thin Solid Films* **515**, 6285 (2007).
21. R. Schlaf, H. Murata, Z.H. Kafafi, *J. Electron Spectroscopy and Related Phenomena* **120**, 149 (2001).
22. M.G. Helander, M.T. Greiner, Z.B. Wang, W.M. Tang, Z.H. Lu, *J. Vac. Sci. Technol. A* **29**, 011019 (2011).
23. Ch. Song, H. Chen, Y. Fan, J. Luo, X. Guo, X. Liu, *Appl. Phys. Express* **5**, 041102 (2012).
24. P. Prunici, F.U. Hamelmann, W. Beyer, H. Kurz, H. Stiebig, *J. Appl. Phys.* **113**, 12310 (2013).
25. *CRC Handbook of Chemistry and Physics* (version 2008).
26. Y.H. Heo, D.J. Youn, H. Lee, S. Lee, H.-Min Lee, *Sol. Energ. Mater. Sol. C.* **122**, 107 (2014).
27. S.J. Fonash, *Solar Cell Device Physics* (Elsevier Inc., Second Edition: 2010).
28. Sh.S. Li, *Semiconductor Physical Electronics* (Plenum Press: 1993).
29. Y. Liu, Y. Sun, W. Liua, J. Yao, *Phys. Chem. Chem. Phys.* **16**, 15400 (2014).